Skeletal Radiology (2019) 48:897–905
https://doi.org/10.1007/s00256-018-3085-3

SCIENTIFIC ARTICLE

CT, conventional, and functional MRI features of skull lymphoma: a series of eight cases in a single institution

Zhen Xing[1] · Hongjie Huang[1] · Zebin Xiao[1] · Xiefeng Yang[1] · Yu Lin[1] · Dairong Cao[1]

Received: 13 June 2018 / Revised: 23 September 2018 / Accepted: 26 September 2018 / Published online: 11 October 2018

Abstract

Objective With the hypothesis that the combination of CT, conventional, and functional MRI can indicate a possible diagnosis of skull lymphoma, this study aimed to systematically explore CT, conventional, and functional MRI features of this rare entity.

Materials and methods This retrospective study included eight patients with pathologically confirmed skull lymphomas. CT and conventional MRI findings, including the location, size, attenuation/signal intensity, cystic/necrosis, hemorrhage, calcification, enhancement, skull change, brain parenchyma edema and adjacent structure invasion, were reviewed. We also reviewed multi-parametric functional MR imaging features obtained from diffusion-weighted imaging (DWI, $n = 4$), susceptibility-weighted imaging (SWI, $n = 3$) and dynamic susceptibility-weighted contrast-enhanced perfusion-weighted imaging (DSC-PWI, $n = 1$).

Results The eight patients in this series consisted of five males and three females, with a mean age of 51.1 years. All skull lymphomas showed the tumors extending to extra- and intra-cranial spaces with permeative destruction of the intervening skull. Intratumoral cystic/necrosis was seen in one case. Hemorrhage or calcification was absent. Dural mater infiltration was detected in all cases. Two clivus lymphomas encased internal carotid artery without narrowing the lumen. Three cases invaded brain parenchyma with moderate edema. The tumors demonstrated high signal on DWI with low ADC values comparing to muscles. SWI images showed little intratumoral hemorrhage and vessel. Low relative cerebral blood volume (rCBV) value was detected.

Conclusions Skull lymphomas commonly presented as a homogenous solid tumor extending either intra- or extra-cranially with permeative bone destruction. Restricted diffusion, little intratumoral susceptibility signal, and lower perfusion may indicate a specific diagnosis. Multi-parametric functional MRI may be a promising tool for the diagnosis of skull lymphomas.

Keywords Skull lymphoma · DWI · DSC-PWI · SWI

Introduction

Skull lymphoma is an extremely rare presentation in clinical work, particularly in the case of primary lymphoma [1–3]. Skull lymphoma cannot be easily differentiated from other skull-involved diseases [4–6]. To date, few case reports describing computer tomography (CT) and conventional magnetic resonance imaging (MRI) findings of skull lymphomas have been published [1–15]. However, the imaging findings are yet to be elucidated, and a reliable preoperative diagnosis of this rare entity is still challenging.

Multi-parametric functional MR techniques, including diffusion-weighted imaging (DWI), susceptibility-weighted imaging (SWI), and dynamic susceptibility-weighted contrast-enhanced perfusion-weighted imaging (DSC-PWI), may reflect the characteristics of tumor microenvironment and provide more physiological information than CT and conventional MRI [16, 17]. DWI could assess the Brownian motion of water molecules in the microscopic tissue environment with the quantification of apparent diffusion coefficient (ADC) [17–19]. Recently, Tu et al. [20] has reported that the diagnostic accuracy in differentiating malignant from benign skull-involved lesions could be significantly improved by adding DWI to CT and conventional MRI. SWI could maximize susceptibility difference among various tissues, which may be very helpful in depicting hemorrhagic components, calcifications, or biologic metal accumulation [16, 17, 21].

Zhen Xing and Hongjie Huang contributed equally to this work.

✉ Dairong Cao
dairongcao@163.com

[1] Department of Radiology, First Affiliated Hospital of Fujian Medical University, 20 Cha-Zhong Road, Fuzhou 350005, Fujian, China

DSC-PWI is a relatively novel imaging technique that allows in vivo imaging of tumor microcirculation and vascularity [16, 17]. Nowadays, DWI, SWI, and DSC-PWI have been used to differentiate primary central nervous system lymphomas (PCNSLs) from glioblastomas [16]. However, no previous study which applied multi-parametric functional MR imaging, including DWI, SWI, and DSC-PWI, to diagnose skull lymphomas has been reported.

We hypothesized that the combination of CT, conventional, and functional MRI can indicate a possible diagnosis of skull lymphoma. Thus, the first purpose of this study was to investigate CT and conventional MRI findings of skull lymphomas with a relatively large sample size. Additionally, multi-parametric functional MRI features of skull lymphomas obtained from DWI, SWI, and DSC-PWI were also systematically evaluated.

Materials and methods

Patients

This retrospective study was approved by the institutional review board of our hospital and the patient informed consent was waived. Patients were identified from the case records from June 2005 to May 2017 in our hospital. The inclusion criteria were as follows: (1) histopathological diagnosis of skull lymphoma; (2) CT and (or) MR examination was performed; (3) sufficient imaging quality for diagnosis. The exclusion criteria were patients who received treatment (surgery, chemotherapy, or radiation therapy) before CT and MRI examinations. A total of 11 potential patients were identified from case records. Two patients were excluded due to no imaging database. One patient who received surgical resection previously was also excluded. Ultimately, eight patients met the criteria and were included into this study. All patients underwent MR examinations; six patients underwent CT scans at the same time. The clinical, radiological, and pathological data were also reviewed.

CT and MR imaging protocol

The CT examinations were performed with a 16-detector row helical CT scanner (Aquilion, Toshiba Medical Systems, Japan, $n = 3$) or a 320-detector volume CT scanner (Aquilion ONE, Toshiba Medical Systems, Japan, $n = 3$). The scan parameters were as follows: 1- to 5-mm section thickness, 120-kV voltage, 200- to 300-mA current, and 512 × 512 matrix.

Three patients were performed on a 0.5-Tesla MR system (Flexart, Toshiba Medical Systems, Japan), two patients were performed on a 1.5-Tesla MR system (Signa Infinity Twinspeed, GE Medical Systems, USA), and three patients were performed on a 3.0-Tesla MR system (Magnetom Verio TIM; Siemens Healthcare, Germany).

The protocols of 0.5-Tesla MR system consisted of the following sequences: transverse T1-weighted imaging (T1WI, TR/TE = 500/15 ms), transverse T2-weighted imaging without fat-suppression (T2WI, TR/TE = 4000/100 ms), and three-planes contrast-enhanced T1-weighted imaging (CE-T1WI, TR/TE = 500/15 ms) were obtained after intravenous injection of gadopentetate dimeglumine (Gd-DTPA) at a dosage of 0.1 mmol/kg of body weight.

The protocols of 1.5-Tesla MR system included the following sequences: transverse and sagittal T1WI (TR/TE = 540/20 ms), transverse T2WI without fat-suppression (TR/TE = 4000/108 ms), transverse T2 fluid-attenuated inversion recovery (T2-FLAIR, TR/TE = 8600/120 ms, TI = 2100 ms), transverse DWI (TR/TE = 6000/85.5 ms, Average = 2, b value = 0 and 1000 s/mm^2) and three-planes CE-T1WI (TR/TE = 540/20 ms) were obtained after intravenous injection of Gd-DTPA.

The sequence parameters on 3.0 T MR system were as follows: transverse and sagittal T1WI (TR/TE = 250/2.5 ms), transverse T2WI without fat-suppression (TR/TE = 6000/96 ms), transverse T2-FLAIR (TR/TE = 7000/94 ms, TI = 2500 ms), transverse DWI (TR/TE = 8200/102 ms, number of average = 1, b value = 0 and 1000 s/mm^2) and three-planes CE-T1WI (TR/TE = 250/2.5 ms) were obtained after intravenous injection. In addition, SWI was available in three patients and DSC-PWI was performed in one patient.

SWI was performed on a cross-section with a 3D fully flow-compensated gradient-echo sequence with the following parameters: TR/TE = 27/20 ms, flip angle = 15°, FOV = 220 × 220 mm, matrix = 256 × 256, number of excitation (NEX) = 1, section thickness = 1.5 mm, intersection gap = 0.3 mm. Subsequently, the SWI sequences were reconstructed with the minimum intensity projection (MinIP) technique to obtain images with a section number, thickness, and position similar to other sequences.

DSC-PWI was performed with a gradient-recalled T2*-weighted echo-planar imaging sequence before CE-T1WI. The imaging parameters were as follows: TR/TE = 1000/54 ms, flip angle = 35°, NEX = 1.0, FOV = 220 × 220 mm, slice thickness = 5 mm, and intersection gap = 1.0 mm. During the first three phases, images were scanned before injecting the contrast agent to establish a precontrast baseline. When the scan was to the fourth phase of DSC-PWI, 0.1 mmol/kg body weight of Gd-DTPA was injected with an MR-compatible power injector at a rate of 5 ml/s through an intravenous catheter placed in the antecubital vein, followed immediately by a 20-ml continuous saline flush. The series of 20 sections, 60 phases, and 1200 images were acquired in 96 s.

Imaging analysis

Two experienced neuroradiologists who were blinded to the patients' clinical and pathological data independently evaluated CT and conventional MRI features, including location,

size, attenuation/signal intensity, cystic/necrosis, hemorrhage, calcification, enhancement, skull change, brain parenchyma edema, adjacent structure invasion, and disagreements were resolved by consensus.

For tumor size, the three orthogonal maximal diameters were measured. Lesion attenuation characteristics were classified as low, iso, or high density relative to semispinalis capitis and brain grey matter. Signal intensity was graded as low, iso, or high signal intensity relative to semispinalis capitis and brain grey matter on the T1- and T2WI. Cystic/necrosis components were defined as areas that appeared hypointense on T1WI, hyperintense on T2WI, and no enhancement on post-gadolinium T1WI sequences. Hemorrhage was defined when the CT attenuation values fell in the range of 50–90 Hu on nonenhanced scans, or short T1- and long T2-signal on MR images, and no enhancement on post-contrast images. The presence of calcification was confirmed according to nonenhanced CT and SWI. Patterns of enhancement were evaluated by extent as follows: none, focal (less than 1/4 of the mass), partial (between 1/4 and 3/4), homogeneous (more than 3/4) or rim (peripheral enhancement). The degree of enhancement was graded as none, minimal-to-mild, or moderate-to-marked (similar enhancement to normally enhanced choroid plexus) [22]. The cortical changes were classified as follows: absent, permeative destruction (fine linear or tiny hole destructive pattern of intracortical, without disturbance of cortical integrity), cortical destruction (normal cortical bone completely or partially replaced, with disturbance of cortical integrity), or cortical osteosclerosis (thickening of cortical, without intensity or signal abnormalities) [23, 24]. Brain parenchyma edema was graded as follows: absent, mild (extending < 1 cm from the outer margin of the mass), moderate (between 1 and 4 cm) or severe (> 4 cm) [25]. Adjacent structure invasion was assessed including vessel, dura mater, and brain parenchyma invasion.

The DWI signal intensity was evaluated relative to normal semispinalis capitis. We defined restricted diffusion of skull lymphomas as ADC values lower than that of muscles, while non-restricted diffusion as ADC values higher than that of muscles [26].

The degree of intratumoral susceptibility signals included four grades on SWI as previously described [27]: grade 0: no hemorrhage or vessel, grade 1: 1–10 dot-like hemorrhage or 1–5 intralesional vessels, grade 2: 11–20 dot-like hemorrhage or 6–10 intralesional vessels, grade 3: more than 20 dot-like hemorrhage or more than ten intralesional vessels.

DSC-PWI signal intensity was evaluated using relative cerebral blood volume (rCBV). Degree of rCBV was categorized as low (lower or equal to normal brain parenchyma), high (greater than normally post-contrast choroid plexus), and moderate (rCBV between low and high).

For the quantitative assessment of DWI and DSC-PWI data, ADC and rCBV values were measured by manually placing the region of interest (ROI) inside the tumor regions. The ROIs were placed on the enhancing solid portion of the tumors corresponding to CE-T1WI, taking care of to avoid hemorrhage, necrotic, and cystic areas. At least five uniform small round ROIs with sizes of approximately 30-40 mm^2 were selected to place inside the tumors on the ADC and DSC perfusion images, and average ADC and rCBV value were obtained.

Results

Clinical findings

The five men and three women in this study had a mean age of 51.1 years (range, 28-68 years). Seven cases were single tumors and one case showed two tumors, with nine tumors in total. Clinical records of eight patients were reviewed and the findings summarized in Table 1. The most prevalent complaint was subcutaneous mass (6/8, 75.0%). Headache was observed in three patients (3/8, 37.5%), and focal neurological deficit was observed in two patients (2/8, 25.0%). Combined with chest and abdomen imaging, bone marrow biopsy, and clinical follow-up, five cases were deemed to primary lymphomas and three were deemed to secondary lymphomas.

Imaging findings

CT and conventional MRI features of skull lymphomas are summarized in Table 2. Six are cases located in the cranial vault without predilection sites. Two skull base lymphomas were both located in the clivus. The size of lymphomas in the cranial vault seemed to be larger than that in the skull base.

Comparing with muscles, the solid components of tumors presented as isodense ($n = 4$) and hyperdense ($n = 2$) on the non-contrast CT; hypointense ($n = 2$) and isointense ($n = 6$) on T1WI; isointense ($n = 2$) and hyperintense ($n = 6$) on T2WI. Comparing with grey matter, the solid components of tumors presented as isodense ($n = 1$) and hyperdense ($n = 5$) on the non-contrast CT; hypointense ($n = 2$), isointense ($n = 4$), and hyperintense ($n = 2$) on T1WI; hypointense ($n = 2$), isointense ($n = 2$) and hyperintense ($n = 4$) on T2WI. Seven cases demonstrated homogeneous enhancement without necrosis, hemorrhage, or calcification. Cystic/necrosis was found in one lesion. The degree of enhancement was minimal-to-mild in two cases and moderate-to-marked in six cases.

All cases exhibited permeative bone destruction, and one lesion was accompanied by osteosclerosis meanwhile. Thickened and enhanced dura mater was detected in all cases. Three tumors infiltrated brain parenchyma with moderate parenchyma edema (Fig. 1). Two clivus lymphomas involved internal carotid artery, which encased the vessels without narrowing of the lumen (Fig. 2).

Table 1 Clinical features of skull lymphomas

No.	Sex/age	Symptoms	Primary or secondary	Number	Location	Size
1	M/53	Subcutaneous mass, headache	Primary	One	Bilateral parietal	8.2 × 6.7 × 6.0
2	M/28	Subcutaneous mass	Primary	One	Right occipital	5.0 × 4.6 × 5.5
3	F/68	Subcutaneous mass, headache	Primary	One	Left fronto-tempo-parietal	3.7 × 6.3 × 6.1
4	M/39	Subcutaneous mass	Primary	Two	Left fronto-parietal/right fronto-parietal	2.6 × 11.2 × 3.1/ 4.5 × 5.8 × 3.3
5	F/68	Subcutaneous mass	Secondary	One	Bilateral frontal	5.0 × 3.2 × 2.8
6	M/45	Subcutaneous mass, headache, blurred vision	Primary	One	Bilateral parieto-occipital	6.7 × 10.4 × 5.8
7	F/62	Diplopia	Secondary	One	Clivus	2.3 × 2.2 × 2.3
8	M/46	Diplopia, ptosis	Secondary	One	Clivus	3.5 × 2.9 × 2.1

M, male; F, female

DWI was available in four patients. Four tumors showed high signal in DWI with low ADC values comparing to muscles. The mean ADC values were $(0.51 \pm 0.07) \times 10^{-3}$ mm^2/s, ranging from 0.45-0.61 $\times 10^{-3}$ mm^2/s. SWI manifested six dot-like hemorrhage and five short line-like intratumoral vessels in one lesion, which graded into 1 (Fig. 1). However, inhomogeneous magnetic field of skull base caused obvious artifact in two clivus cases. DSC-PWI was available in one case; the tumor showed low perfusion with the rCBV value of 1.32. (Fig. 1).

Pathology findings

Six cases were completely or partially resected, and biopsy was performed in another two patients. All cases were pathologically confirmed as B cell non-Hodgkin lymphoma (NHL). Immunohistochemical staining was performed in seven cases and confirmed as diffuse large B cell lymphoma (DLBCL). Microscopically, the tumors consisted of diffuse large lymphoid cells with large nucleoli and scanty cytoplasm. Immunohistochemical analysis of seven DLBCLs showed that the tumors were positive for CD20 (+, 7/7), CD79a (+, 5/7), BCL-2 (+, 4/7), Mum-1 (+, 2/7), Ki-67 (+, 5/7, 40%-90%). All seven cases were negative for CD3.

Discussion

Skull lymphoma has been considered as an extremely rare presentation. In our cohort, skull lymphomas manifested no marked gender difference and occurred commonly in the older, which was consistent with a previous study [4]. The clinical complaints were varied. Subcutaneous masses were relatively large and most commonly seen in cranial vault lymphomas, which were in good agreement with previous reviews [2, 4]. As for skull base lymphomas, the complaints were nonspecific. Two cases in our study presented with eye discomfort due to involved cranial nerve paralysis. Because of the biological behavior of skull base lymphomas, such as deep location and easy infiltration to adjacent cranial nerve, the clinical manifestations of skull base lymphoma may be earlier and more obvious than that of cranial vault entity. In addition, this also explained why skull base lymphomas were relatively smaller than cranial vault tumors in our cohort.

Due to the hypercellularity of lymphoma [28], it was not surprising that skull lymphomas could manifest as isodense or hyperdense on precontrast CT images, and showed iso-hypointense on T1WI and iso-hyperintense on T2WI comparing to the muscles in our series, but these nonspecific CT and conventional MRI appearances contributed little to differentiate skull lymphomas from other skull-involved diseases. Tumoral cystic/necrosis is usually caused by inadequate blood supplement and may suggest more progressive stages of the diseases. Our study found that cystic/necrosis was rarely seen before treatment and was only found in one mass of nine, which were similar to the results reported previously [29].

Both cranial vault and skull base lymphomas exhibited permeative destruction in the intervening skull, which was in good agreement with those previously described [8, 9]. In the early stages, the involved skull usually shows a moth-eaten pattern and minimal cortical destruction, without disturbance of cortical integrity. The reason of permeative destruction is not well understood, but is most likely associated with the following processes: lymphoma cells infiltrated the intradiploe space by extending along the emissary veins, and bone marrow was replaced by tumor cells [8]. Thus, the involved skull could be a distinguishable sign to characterize skull lymphoma. On post-gadolinium T1WI, the involved skull showed mild heterogeneous enhancement, which implied tumoral cells invasion. In our study, two clivus lymphomas demonstrated relatively small lesions and remarkable medullary destruction, reflecting progressed stage or aggressive nature of secondary skull lymphomas. However, it should also be noted that tumoral cells of lymphoma could gradually extend and

Table 2 Conventional imaging features of skull lymphomas

No.	Imaging findings comparing with muscles			Imaging findings comparing with grey matter			Cystic/ necrosis	Hemorrhage/ calcification	Patterns/degree of enhancement	Skull change	Brain parenchyma edema	Adjacent structure invasion
	CT	T1WI	T2WI	CT	T1WI	T2WI						
1	Hyperdense	Isointense	Hyperintense	Hyperdense	Isointense	Hyperintense	Yes	No	Heterogeneous, moderate-to-marked	Permeative	Moderate	Dura mater, brain parenchyma
2	Hyperdense	Isointense	Hyperintense	Hyperdense	Isointense	Hyperintense	No	No	Homogeneous, moderate-to-marked	Permeative	Moderate	Dura mater, brain parenchyma
3	NA	Hypointense	Hyperintense	NA	Hypointense	Hyperintense	No	No	Homogeneous, moderate-to-marked	Permeative	None	Dura mater
4	Isodense	Isointense	Hyperintense	Isodense	Isointense	Isointense	No	No	Homogeneous, moderate-to-marked	Permeative	None	Dura mater
5	Isodense	Isointense	Hyperintense	Hyperdense	Isointense	Isointense	No	No	Homogeneous, minimal-to-mild	Permeative, osteosclerosis	None	Dura mater
6	Isodense	Hypointense	Hyperintense	Hyperdense	Hypointense	Hyperintense	No	No	Homogeneous, moderate-to-marked	Permeative	Moderate	Dura mater, brain parenchyma
7	NA	Isointense	Isointense	NA	Hyperintense	Hypointense	No	No	Homogeneous, minimal-to-mild	Permeative	None	Dura mater, ICA
8	Isodense	Isointense	Isointense	Hyperdense	Hyperintense	Hypointense	No	No	Homogeneous, moderate-to-marked	Permeative	None	Dura mater, ICA

ICA internal carotid artery

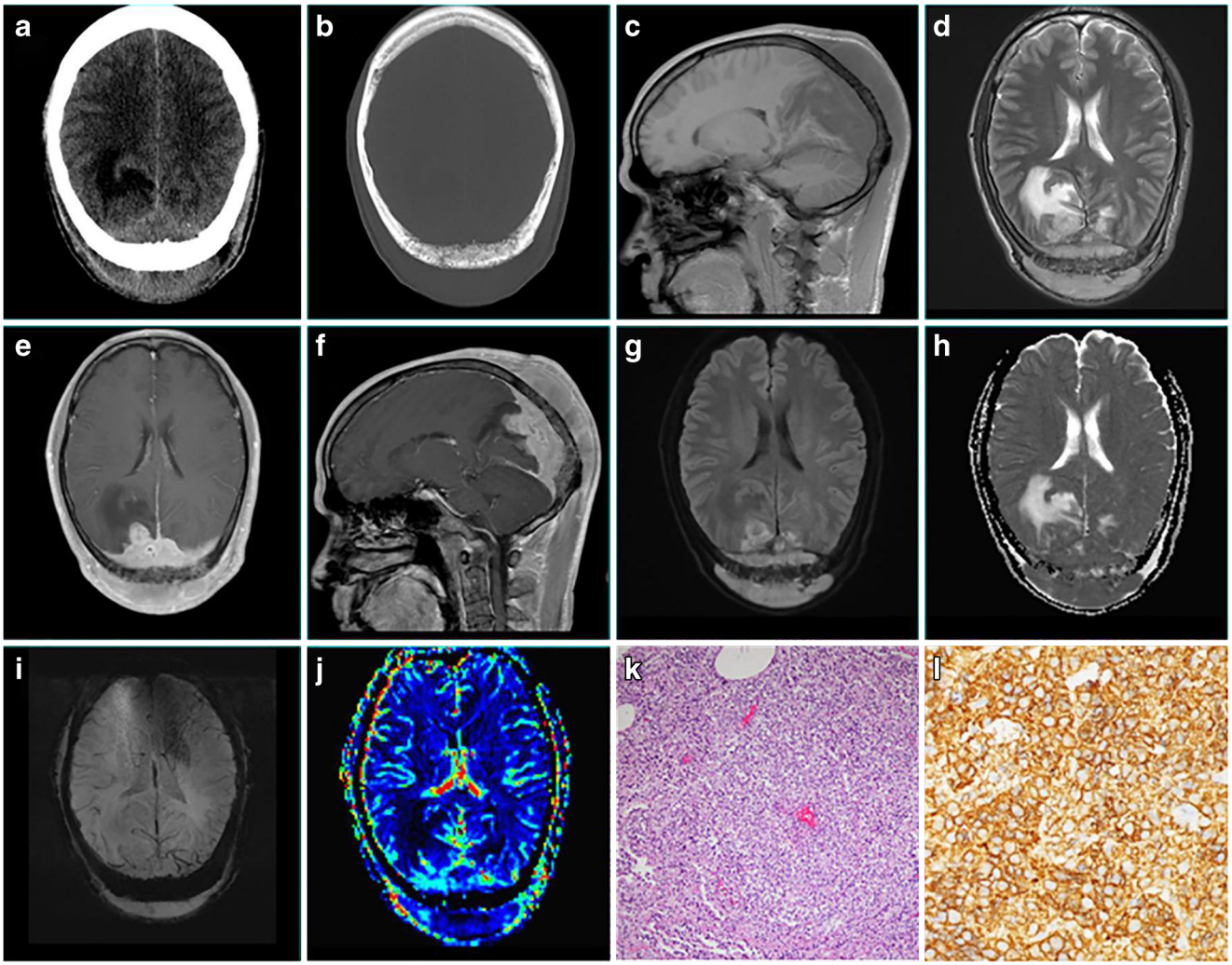

Fig. 1 A 45-year-old man with primary skull diffuse large B-cell lymphoma (case six). **a** CT scan of the brain window and **b** bone window demonstrates a bilateral parieto-occipital isodense lesion involving brain parenchyma with permeative destruction. **c, d** Pre-contrast MRI reveals an intra- and extra- cranial mass as hypointense on T1WI and hyperintense on T2WI, involving the occipital lobes with moderate parenchyma edema. **e, f** Post-contrast MRI demonstrates a homogeneously enhanced mass with dural tail sign **g, h** DWI shows hyperintense with low ADC values comparing to muscles. **i** SWI-MinIP shows little dot-like hemorrhage and intralesional vessels. **j** Pathological observation demonstrates diffuse lymphoid cells infiltration (HE, ×100). **k** Immunohistochemical staining shows CD20-positive tumoral cells

finally replace the cortical with the disease progressing [3], making it difficult to differentiate from other malignant skull–involved masses.

Skull lymphomas are highly malignant tumors and adjacent structures invasions are common. Post-contrast enhanced T1WI are superior in delineating the tumor extension. Dural mater infiltration, manifesting as diffuse thickening and enhancement of adjacent dura, was most commonly seen, which is similar to dural tail sign. This finding is probably due to the infiltration of lymphoma cells and reactive edema, which resulted in difficulties for complete tumor resection [9]. Similar to the previous study [10], encasement of vessels without obvious narrowing was found in two skull base lymphomas in our present study. This sign also indicates the characteristic of permeative growth pattern. Other cavernous sinus infiltrative lesions, such as meningioma and metastasis, usually manifest compression effect to the vessels, which was different from the skull lymphomas.

We especially evaluated multi-parametric functional MR imaging findings of skull lymphomas, which have not been systematically described in previous studies. DWI could non-invasively evaluate the tumor cellularity with the measurement of ADC values [17–19]. The ADC values in the range of 0.51 to 0.59×10^{-3} mm^2/s have been reported for lymphomas in the skull base region, which was significantly lower than skull base osteomyelitis and nasopharyngeal carcinomas [19, 30]. In our group of skull lymphomas, the mean ADC values were $0.51 \pm 0.07 \times 10^{-3}$ mm^2/s, which were similar to the previous study. This feature may be associated with the factors that lymphoma is a hypercellular tumor with large lymphoid cells and little extracellular matrix [28]. It has also been reported that lymphoma has lower ADC values

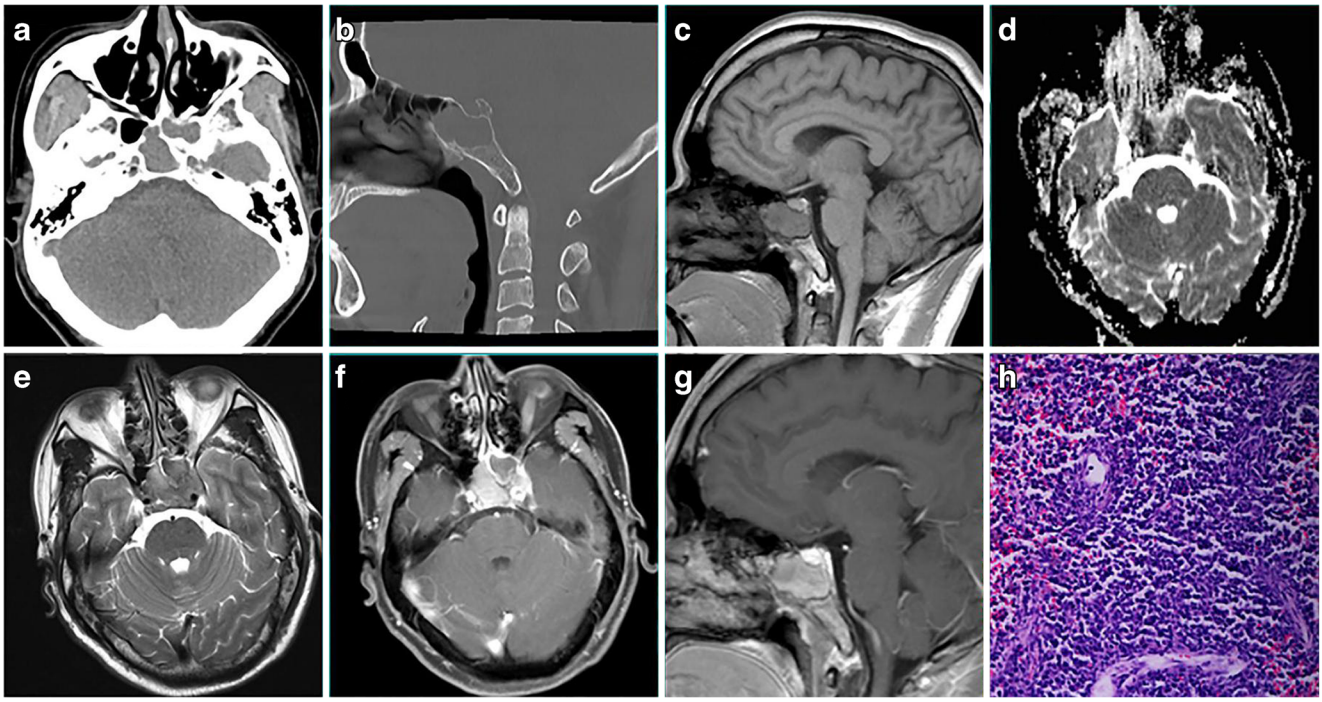

Fig. 2 A 46-year-old man with secondary clivus diffuse large B cell lymphoma (case eight). **a** Axial cranial CT shows a slightly hyperdense mass. **b** Bone window CT and **c** sagittal T1WI show permeative destruction, and marrow cavity is destroyed completely. **d** DWI reveals low ADC values. **e** T2WI shows a homogenous isointense tumor. **f, g** Post-gadolinium T1WI shows marked and homogeneous enhancement. The bilateral cavernous sinuses are infiltrated, and carotid arteries are encased by the tumor without narrowing. **h** Pathological observation shows a diffuse, highly cellular blastic infiltrate consisting of large lymphoid tumor cells with large nucleoli and scanty cytoplasm (HE, ×200)

compared with other malignant tumors [31, 32]. Therefore, DWI may be a promising tool in differentiating skull lymphoma from other skull benign and malignant tumors.

SWI is extraordinarily sensitive to magnetic susceptibility effects, making it superior for the detection of microhemorrhage and neovascularity [16, 17, 21]. Our study revealed little hemorrhage and intralesional vessel number detected by SWI images, probably because lymphoma is scarce in tumor neovascularization compared with other malignant tumors [33, 34]. The lack of significant necrosis and hemorrhage is another distinguishable sign for the characterization of skull lymphomas. Thus, we assumed that SWI images can enhance diagnostic confidence for the skull lymphoma. Unfortunately, artifact caused by gas and bone limited the use of SWI, especially in skull base lesions.

DSC-PWI, a relatively novel technique that can noninvasively provide direct insight into the microvascular information, is applied for the diagnosis of intra- and extra-axial tumors [16, 17]. It has been reported that rCBV values showed good correlations with angiographic vascularity [35]. Lymphoma is characterized by the angiocentric growth and tumor cells tend to cluster around pre-existing vessels [33], suggesting that lymphoma is scarce in tumor neovascularization. Our limited case of skull lymphomas confirmed this histological basis and manifested low perfusion. Given that most of common skull-involved tumors, including metastasis, meningioma, and plasmacytoma, have abundant blood supplies; DSC-PWI may be very helpful in differentiating lymphoma from other skull-involved hypervascular tumors.

Skull lymphomas should be differentiated from other solid skull-involved tumors, including metastases, meningiomas, plasmacytomas, and aggressive pituitary adenomas. Skull metastases typically manifest heterogeneous soft-tissue masses with clear cortical destruction [4, 6]. A history of malignancy plays an important role in the diagnosis. Furthermore, skull metastases usually show high rCBV values on DSC-PWI and diffuse intratumoral susceptibility signals on SWI. Meningiomas usually appear as soft-tissue masses with osteosclerosis. The cavity would be narrow or displaced when the vessel is wrapped. Moreover, most subtypes of meningiomas are hypervascular tumors with high rCBV values [35]. Plasmacytomas, as small round cell tumors, show subtle bone erosions and restricted diffusion on DWI images, which is similar to skull lymphomas [28, 36]. DSC-PWI is highly recommended because plasmacytomas are highly vascular tumors [36]. Aggressive pituitary adenomas occasionally appear as a large homogenous mass involving the skull base and encasing vessels without obvious narrow, which may mimic a lymphoma. Unlike skull lymphomas, aggressive pituitary adenomas exhibit iso-high ADC values owing to its collagen content [37].

The principal limitation was the small sample size of multi-parametric functional MRI techniques due to its extremely rare occurrence. Although the number evaluated was limited, these findings could be explained by the histopathological features of skull lymphomas. To draw more definite conclusions, further studies with a large sample size are needed.

Conclusions

In conclusion, skull lymphomas generally demonstrate as solid tumors which extend either intra- or extra-cranially with permeative bone destruction. Intratumoral cystic/necrosis hemorrhage, or calcification is uncommon. Restricted diffusion, little intratumoral susceptibility signal and lower perfusion may indicate a specific diagnosis. Multi-parametric functional MRI may be helpful for the diagnosis of skull lymphomas.

Authors' contributions Z.X. carried out the statistical analyses and image post-processing. H.H. performed the study and drafted the manuscript. Z.X. and X.Y. performed the scanning sequences. Y.L. analyzed the case histories. D.C. conceived the study idea, participated in its design, and helped in drafting the manuscript. All authors read and approved of the final manuscript.

Funding This study was funded by the Leading Project of the Department of Science and Technology of Fujian Province (No. 2016Y0042), and the Special Funds of Provincial Finance of Fujian Province (No. BPB-CDR2013).

Compliance with ethical standards

Conflict of interest The authors declare that they have no conflicts of interest.

Ethical approval All procedures performed in the studies involving human participants were in accordance with the ethical standards of the institutional and local Ethical Committee, and with the 1964 Helsinki Declaration and its later amendments. For this type of study formal consent is not required.

Informed consent For this type of study formal consent is not required.

References

1. Hans FJ, Reinges MH, Nolte K, Reipke P, Krings T. Primary lymphoma of the skull base. Neuroradiology. 2005;47(7):539–42.
2. El Asri AC, Akhaddar A, Baallal H, et al. Primary lymphoma of the cranial vault: case report and a systematic review of the literature. Acta Neurochir. 2012;154(2):257–65.
3. Fukushima Y, Oka H, Utsuki S, Nakahara K, Fujii K. Primary malignant lymphoma of the cranial vault. Acta Neurochir. 2007;149(6):601–4.
4. Da RA, Da RT, Da SC, et al. Cranial vault lymphoma: a systematic review of five patients. J Neuro-Oncol. 2010;100(1):9–15.
5. Muin IA, Saffari HM, Hasimah YN. Primary non-Hodgkin's lymphoma of the cranial vault mimicking a meningioma: a case report. Med J Malaysia. 1997;52(1):86–8.
6. Wang L, Lin S, Zhang J, Wang C. Primary non-Hodgkin's lymphoma of the skull base: a case report and literature review. Clin Neurol Neurosurg. 2013;115(2):237–40.
7. Ko MJ, Hwang SN, Park YS, Nam TK. Primary malignant lymphoma of the cranial vault with extra- and intracranial extension. Brain Tumor Res Treat. 2013;1(1):32–5.
8. Tashiro R, Kanamori M, Suzuki H, et al. Diffuse large B cell lymphoma of the cranial vault: two case reports. Brain Tumor Pathol. 2015;32(4):275–80.
9. Choi HK, Cheon JE, Kim IO, et al. Central skull base lymphoma in children: MR and CT features. Pediatr Radiol. 2008;38(8):863–7.
10. Jung C, Zimmermann M, Seifert V. Clivus lymphoma. Acta Neurochir. 2004;146(5):533–4.
11. Nakamura A, Toyoda K, Shozawa Y, et al. Primary non-Hodgkin lymphoma of the skull base presenting with Garcin syndrome: MRI manifestations. J Neuroimaging. 2009;19(3):295–7.
12. Aronson PL, Reilly A, Paessler M, Kersun LS. Burkitt lymphoma involving the clivus. J Pediatr Hematol Oncol. 2008;30(4):320–1.
13. Ochiai H, Kawano H, Miyaoka R, et al. Primary diffuse large B-cell lymphomas of the temporoparietal dura mater and scalp without intervening skull bone invasion. Neurol Med Chir. 2010;50(7):595–8.
14. Han MH, Chang KH, Kim IO, Kim DK, Han MC. Non-Hodgkin lymphoma of the central skull base: MR manifestations. J Comput Assist Tomogr. 1993;17(4):567–71.
15. Isla A, Alvarez F, Gutiérrez M, et al. Primary cranial vault lymphoma mimicking meningioma. Neuroradiology. 1996;38(3):211–3.
16. Kickingereder P, Wiestler B, Sahm F, et al. Primary central nervous system lymphoma and atypical glioblastoma: multiparametric differentiation by using diffusion-, perfusion-, and susceptibility-weighted MR imaging. Radiology. 2014;272(3):843–50.
17. Haldorsen IS, Espeland A, Larsson EM. Central nervous system lymphoma: characteristic findings on traditional and advanced imaging. AJNR Am J Neuroradiol. 2011;32(6):984–92.
18. Wu X, Pertovaara H, Dastidar P, et al. ADC measurements in diffuse large B-cell lymphoma and follicular lymphoma: a DWI and cellularity study. Eur J Radiol. 2013;82(4):e158–64.
19. Ozgen B, Oguz KK, Cila A, Diffusion MR. Imaging features of skull base osteomyelitis compared with skull base malignancy. AJNR Am J Neuroradiol. 2011;32(1):179–84.
20. Tu Z, Xiao Z, Zheng Y, et al. Benign and malignant skull-involved lesions: discriminative value of conventional CT and MRI combined with diffusion-weighted MRI. Acta Radiol. 2018:284185118773541.
21. Pinker K, Noebauer-Huhmann IM, Stavrou I, et al. High-field, high-resolution, susceptibility-weighted magnetic resonance imaging: improved image quality by addition of contrast agent and higher field strength in patients with brain tumors. Neuroradiology. 2008;50(1):9–16.
22. Yi KS, Sohn CH, Yun TJ, et al. MR imaging findings of extraventricular neurocytoma: a series of ten patients confirmed by immunohistochemistry of IDH1 gene mutation. Acta Neurochir. 2012;154(11):1973–9.
23. Heyning FH, Kroon HM, Hogendoorn PC, Taminiau AH, van der Woude HJ. MR imaging characteristics in primary lymphoma of bone with emphasis on non-aggressive appearance. Skelet Radiol. 2007;36(10):937–44.
24. Greenfield GB, Warren DL, Clark RA. MR imaging of periosteal and cortical changes of bone. Radiographics. 1991;11(4):611–23.
25. Kim EY, Weon YC, Kim ST, et al. Rhabdoid meningioma: clinical features and MR imaging findings in 15 patients. AJNR Am J Neuroradiol. 2007;28(8):1462–5.

26. Douis H, Davies MA, Sian P. The role of diffusion-weighted MRI (DWI) in the differentiation of benign from malignant skeletal lesions of the pelvis. Eur J Radiol. 2016;85(12):2262–8.
27. Lin Y, Xing Z, She D, et al. IDH mutant and 1p/19q co-deleted oligodendrogliomas: tumor grade stratification using diffusion-, susceptibility-, and perfusion-weighted MRI. Neuroradiology. 2017;59(6):555–62.
28. Krishnan A, Shirkhoda A, Tehranzadeh J, et al. Primary bone lymphoma: radiographic-MR imaging correlation. Radiographics. 2003;23(6):1371–83.
29. Murphey MD, Kransdorf MJ. Primary musculoskeletal lymphoma. Radiol Clin N Am. 2016;54(4):785–95.
30. Maeda M, Maier SE, Sakuma H, Ishida M, Takeda K. Apparent diffusion coefficient in malignant lymphoma and carcinoma involving cavernous sinus evaluated by line scan diffusion-weighted imaging. J Magn Reson Imaging. 2006;24(3):543–8.
31. Fong D, Bhatia KSS, Yeung D, King AD. Diagnostic accuracy of diffusion-weighted MR imaging for nasopharyngeal carcinoma, head and neck lymphoma and squamous cell carcinoma at the primary site. Oral Oncol. 2010;46(8):603–6.
32. Doskaliyev A, Yamasaki F, Ohtaki M, et al. Lymphomas and glioblastomas: differences in the apparent diffusion coefficient evaluated with high b-value diffusion-weighted magnetic resonance imaging at 3T. Eur J Radiol. 2012;81(2):339–44.
33. Koeller KK, Smirniotopoulos JG, Jones RV. Primary central nervous system lymphoma: radiologic-pathologic correlation. Radiographics. 1997;17(6):1497–526.
34. Zhou L, Peng W, Wang C, et al. Primary adrenal lymphoma: radiological; pathological, clinical correlation. Eur J Radiol. 2012;81(3):401–5.
35. Toh CH, Wei KC, Chang CN, et al. Assessment of angiographic vascularity of meningiomas with dynamic susceptibility contrast-enhanced perfusion-weighted imaging and diffusion tensor imaging. AJNR Am J Neuroradiol. 2014;35(2):263–9.
36. Cerase A, Tarantino A, Gozzetti A, et al. Intracranial involvement in plasmacytomas and multiple myeloma: a pictorial essay. Neuroradiology. 2008;50(8):665–74.
37. Lu Y, Xiong J, Geng D, Yin B. Prediction of the consistency of pituitary adenoma: a comparative study on diffusion-weighted imaging and pathological results. J Neuroradiol. 2016;43(3):186–94.